ACS OMEGA

http://pubs.acs.org/journal/acsodf

Article

Biomimetic Growth of Hydroxyapatite in Hybrid Polycaprolactone/Graphene Oxide Ultra-Porous Scaffolds

S. Fuster-Gómez, I. Castilla Cortázar, A. Vidaurre, and A.J. Campillo-Fernández*

Cite This: *ACS Omega* 2023, 8, 7904−7912

Read Online

ACCESS | Metrics & More | Article Recommendations | Supporting Information

ABSTRACT: This paper reports the preparation and characterization of hybrid scaffolds composed of polycaprolactone (PCL) and different graphene oxide (GO) amounts, intending to incorporate the intrinsic characteristics of their constituents, such as bioactivity and biocidal effect. These materials were fabricated by a solvent-casting/particulate leaching technique showing a bimodal porosity (macro and micro) that was around 90%. The highly interconnected scaffolds were immersed in a simulated body fluid, promoting the growth of a hydroxyapatite (HAp) layer, making them ideal candidates for bone tissue engineering. The growth kinetics of the HAp layer was influenced by the GO content, a remarkable result. Furthermore, as expected, the addition of GO neither significantly improves nor reduces the compressive modulus of PCL scaffolds. The thermal behavior of composites was investigated by differential scanning calorimetry, showing an increase in crystallinity as the addition of GO raised, which implies that GO nanosheets can act as seeds to induce the crystallization of PCL. The improved bioactivity was demonstrated by the deposition of an HAp layer on the surface of the scaffold with GO, especially with a 0.1% GO content.

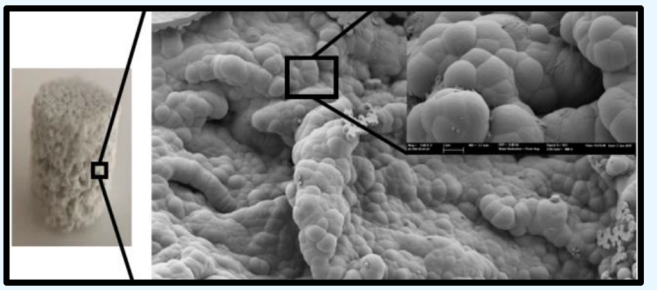

1. INTRODUCTION

Tissue engineering (TE) is an interdisciplinary field that applies the principles of engineering and life sciences to the development of biological substitutes that restore, maintain, or improve the tissue function.[1,2] A common approach proposed in TE is based on the use of porous scaffolds which are temporary three-dimensional structures that provide the necessary support for the cells to proliferate and maintain their differentiated function forming the tissues.[3,4] Scaffolds provide frameworks for cells to attach, proliferate, and form an extracellular matrix (ECM).[5] An ideal scaffold should have the following characteristics: (a) it should be highly porous with an interconnected pore network for cell growth and flow transport of nutrients and metabolic waste; (b) it should be biocompatible and bioresorbable with controllable degradation and resorption rates to match tissue replacement; (c) it should have suitable surface chemistry for cell attachment, proliferation, and differentiation; and (d) it should have mechanical properties to match those of the tissues at the site of implantation.[6−8]

Many approaches in TE have relied on synthetic, biodegradable polymer materials. In addition to having good mechanical properties, the polymers can be manufactured with suitable shapes and geometries to maintain the scaffold's structure during the new tissue formation.[1] PCL is a biocompatible, bioresorbable polyester with certain advantages relative to other polymers such as poly lactic acid. PCL maintains good thermal stability in ambient conditions; it is readily available in large quantities and significantly less expensive. Its ability to process and shape and its tailorable properties such as hydrophobicity, kinetics degradation, and mechanical properties have stimulated extensive research into its potential application in the biomedical field.[6,9−15] Many different fabrication techniques have been proposed to design and develop scaffolds for tissue-engineered implants.[6,10,13,16] The advances of recent years in TE have led to the development of scaffolds, searching for each application's ideal properties using blends and composites. There are several reports of PCL composites using a variety of nanoparticles, such as nano-silica, silver nanoparticles, cellulose nanocrystals, hydroxyapatite (HAp), nano-calcium carbonate, montmorillonite, carbon nanotubes, and derivatives of graphene.[17−24]

Graphene, a synthetic atomic layer of graphite with sp^2-bonded carbon atoms, was described by Boehm et al. in 1986 and isolated and identified by Geim and Novoselov in 2004.[25] GO contains a range of reactive oxygen functional groups, making it a good candidate for use in biomedical applications.[26,27] GO differs from graphene in that it forms a

Received: November 30, 2022
Accepted: January 23, 2023
Published: February 15, 2023

uniform and stable suspension in water, whereas graphene tends to form aggregates. Uniform stable suspension of graphene oxide helps to infiltrate the porous scaffolds, thereby modifying the surfaces of pore walls.[28]

Song et al. fabricated the PCL/GO composite nanofiber scaffolds by electrospinning and studied the effect of the GO concentration on the mechanical properties of PCL/GO nanofiber scaffolds; moreover, they studied the biocompatibility of PCL/GO composite scaffolds in two different cell lines.[29] Two methods were presented to produce covalently linked PCL to the remaining functionalities on the periphery of the graphene sheet using highly reduced, well-dispersed graphene, resulting in graphene/polycaprolactone composites with good mechanical and conducting properties but poor graphene dispersion in the matrix.[30] Several studies[31−36] have shown that the combination of a matrix of PCL reinforced with GO improves the mechanical properties and bioactivity, presenting great potential for biomedical applications.

Both graphene and GO were shown to have an inhibitory effect on the growth of *E. coli*. Akhavan and Ghaderi[37] tested the antibacterial activity of graphene sheets. They verified that direct interaction of the related highly sharp edges with bacteria caused RNA effluxes through the damaged cell membranes of both Gram-negative (*E. coli*) and Gram-positive (*S. aureus*) bacteria.[37] Daulbayev et al.[38] studied the GO/HAp/PCL composite scaffold that showed great antimicrobial activity against Gram-positive and Gram-negative bacterial strains.

Many types of calcium phosphates have been considered as biomaterials for bone reconstruction in dental, orthopedic, and maxillofacial applications due to different behavior in living organisms, including bioactivity, biodegradability, and biological response. Bioactivity, degradation behavior, osteoconductivity, and osteoinductivity of CaP ceramics generally depend on their Ca/P ratio, crystallinity, and phase composition.[39,40] HAp is the most stable among the CaP ceramics; its surfaces provide highly effective nucleating sites for the precipitation of apatite crystals in contact with culture medium and body fluids.[39] The solubility, bioactivity, and biological response of HAp can be modified by anionic and cationic substitution. For these reasons, HAp is widely used for preparing polymer-ceramic composite materials[41,42] to impart bioactivity and osteoconductivity and improve mechanical properties.[43] Kokubo and Takadama[44] proposed that HAp formation in vitro can be produced using a simulated body fluid (SBF) with ion concentrations practically equal to those of human blood plasma. Bohner and Lemaitre[45] proposed an alternative method introducing some differences for improving the reproducibility of the bioactivity test of materials. Other authors have proposed supersaturated SBF formulas, multiplying the concentration of SBF to accelerate the HAp formation.[46−48] A recent review article[49] focused on the development of GO/HAp nanocomposites as potential coating materials that can provide a solution to the rejection of implants.

In previous studies, a series of PCL/GO nanocomposites were produced by the solution mixing method in order to analyze morphological changes, crystallization, molecular weight, and thermal properties according to the GO content.[24] Subsequently, the effect of small amounts of GO on the modulation of degradation at extreme pHs[50] was also explored, as well as the effect of the addition of GO on enzymatic degradation (Pseudomonas lipase).[51]

In this work, highly interconnected porous composite scaffolds composed of PCL as the support material and GO as the filler material have been synthesized using the solvent-casting/particulate leaching method. Bioactivity is a key factor for the success of a biomaterial for clinical applications, so HA deposition onto the material surface makes them ideal candidates for TE applications. The scaffolds were characterized by microscopy and elemental analysis, porosity measurements, mechanical compression tests, and DSC. Subsequently, a concentrated SBF was used to achieve the deposition of a layer of biomimetic HAp on the surface of the materials by immersion, seeking to evaluate the influence of nanometric GO on the growth kinetics of HAp. HAp deposition was determined by energy-dispersive X-ray analysis (EDX) and Fourier-transform infrared spectroscopy (FTIR).

2. MATERIALS AND METHODS

2.1. Preparation of the Scaffolds. Poly (ε-caprolactone), PCL, with a weight-average molecular weight of 43,000−50,000 from Polysciences, 1,4-dioxane from Thermo Fisher Scientific, polyethylmethacrylate spheres of 140−220 μm diameter (Elvacite 2043 acrylic resin, PEMA) from Lucite International, and ethanol 98% from Scharlau were used as received. Graphene oxide powder, GO, from Graphenea, was subjected to pretreatment before use as follows: a 1 mg/mL solution of GO powder/Milli-Q H_2O was subjected to sonication in a Sonopuls ultrasonic homogenizer (Bandelin HD3200) for 2 h operating at 50 W, pulsation time on/off 500/500 ms, respectively, equipped with a TT13FZ probe. The mixture was placed in a glass containing ice that was replaced at 10 min intervals to dissipate the internal heat induced by sonication. The mixture was centrifuged in an Eppendorf 5804R at 14,000 rpm for 25 min. The supernatant was removed, and the precipitate was placed in a petri dish under vacuum at 40 °C for 24 h. Precipitated GO was dispersed in dioxane in a VWR USC600TH Ultrasonic Bath (VWR International) for 20 min.

Scaffolds were prepared by solvent-casting, particulate leaching, and the freeze extraction process. Thus, PCL was dissolved in dioxane under stirring for 24 h at room temperature. The ratio of PCL/dioxane was 17.6%w/w. A constant amount of the PCL/dioxane solution was mixed with different amounts of treated-GO/dioxane dispersion and a constant amount of porogen (PEMA). The mixture was hand-stirred and immediately frozen in liquid nitrogen. Solvent extraction was performed in cold ethanol at −20 °C, which was replaced periodically for a week. Subsequently, the samples were punched to obtain 4 mm in diameter. Finally, porogen was dissolved by immersion in ethanol in a bath at 40 °C for a month. The GO/PCL content in the scaffolds was 0, 0.1, 0.2, and 0.5% by weight. Nanocomposite scaffolds were named sPCL, sPCL-0.1, sPCL-0.2, and sPCL-0.5, respectively.

2.2. Biomimetic HAp Deposition. The bioactivity of the scaffolds was studied throught HAp surface deposition following the the Bohner and Lemaitre method.[45] Briefly, two solutions were prepared: the first one contained NaCl, $NaHCO_3$, KCl, $K_2HPO_4{\cdot}3H_2O$, $MgCl_2{\cdot}6H_2O$, and Na_2SO_4 and the second one contained NaCl and $CaCl_2$, both with 1 M HCl. Thus, the supersaturated SBF was prepared by a factor of 5, 5 × SBF, to accelerate the HAp deposition. The samples were kept in an incubator under a 5% CO_2 atmosphere during the immersion at 37 °C. The scaffolds were immersed in 5 ×

https://doi.org/10.1021/acsomega.2c07656
ACS Omega 2023, 8, 7904−7912

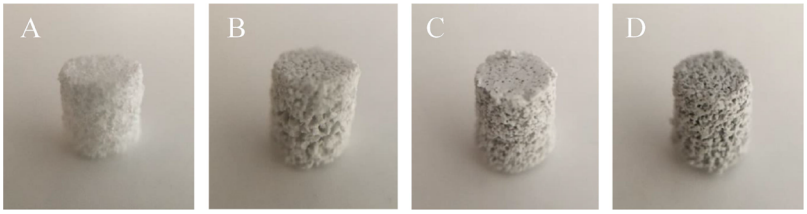

Figure 1. Sample photographs according to the GO content. (A) Neat sPCL, (B) sPCL/GO-0.1, (C) sPCL/GO-0.2, and (D) sPCL/GO-0.5.

SBF for 12 and 72 h and rinsed with ultrapure Milli-Q water for subsequent analysis.

2.3. Visual Examination, Field Emission Scanning Electron Microscopy (FESEM), EDX Analysis, and Transmission Electron Microscopy (TEM). Photographs for visual examination were taken using smartphone macro lenses. Before and after immersion in SBF, the sample morphology was characterized on a ZEISS Ultra-55 FESEM (Zeiss Oxford Instruments, Abingdon, UK). The samples were frozen cryogenically using liquid nitrogen and sectioned longitudinally. Subsequently, they were subjected to vacuum for total solvent removal. The samples studied after immersion in 5 × SBF were gently washed with Milli-Q water, allowed to dry partially at room temperature, and maintained under vacuum to ensure complete water evaporation. In this case, cryogenization was not carried out, avoiding possible detachment of the calcium phosphate crystals formed on the surface of the samples. The scaffolds were placed on a copper stub and sputtered with platinum in the case of FESEM and carbon in the case of EDX analysis. The extra high tension (EHT) was set between 1 and 2 kV for micrographs and 10 kV for EDX analysis at a working distance of 10 mm. EDX allowed to obtain the elementary composition of the sample qualitatively and quantitatively in order to study the calcium/phosphorus (Ca/P) ratio after the growth of HAp on the surface. For GO visualization, GO was ultra-diluted in water and sonicated in a VWR USC600TH Ultrasonic Bath (VWR International) for 10 min. Then, a drop of GO/H_2O was placed on a copper grid until the water was evaporated. Images were taken by the JEOL JEM-1010 transmission electron microscope at 100 kV.

2.4. Porosity Measurements. The porosity was obtained by the gravimetric method through Archimedes' principle. A Mettler Toledo, AE 240 semi-microbalance with a readability of 0.01 mg equipped with a Mettler ME 33360 accessory kit was used to weigh the samples. First, the weight of the dried scaffolds (m_D) was obtained. Then, the scaffolds were inserted into a tube containing ethanol and connected to a vacuum pump to replace the air inside the pores of the scaffolds with ethanol. EtOH-filled scaffolds were weighed (m_W) after removing the excess ethanol from the surface. Finally, EtOH-filled scaffolds were immersed in ethanol and weighed through the accessory kit (m_I). Porosity can be obtained as the ratio between wet and dry weight difference and wet and immersion weight difference, as shown in eq 1.

$$\text{Porosity}\ (\%) = \frac{m_W - m_D}{m_W - m_I} \times 100 \quad (1)$$

2.5. Gel Permeation Chromatography (GPC). GPC was used to determine the molecular weight distribution of the samples using the Waters Breeze GPC 1525 Binary HPLC (Waters Corporation, Milford, MA, USA) equipped with a 2414 refractive index detector and Waters Styragel HR THF columns. Tetrahydrofuran (THF) was used as the eluent with a flow rate of 0.5 mL/min. The injection volume was 50 μL, and two injections of each were made. PCL molecular weights were calculated from the Mark–Houwink–Sakurada parameters ($k = 2.9 \times 10^{-4}$ [dL/g], $\alpha = 0.7$) provided by Huang et al.[52]

2.6. Fourier-Transform Infrared Spectroscopy. The characterization of the different compounds to identify the functional groups present in the samples before and after HAp growth was performed using Bruker's FTIR Alpha equipment in absorbance mode. All measurements were performed by attenuated total reflectance spectroscopy (ATR) with the Smart Multi-Bounce HATR accessory for solids with a KBr crystal. The spectra resulted from the averages of 24 scans at a resolution of 4 cm^{-1} between 400 and 4000 cm^{-1}.

2.7. Mechanical Properties under Compression. The scaffolds were subjected to the uniaxial compression test in order to study the effect of the addition of graphene oxide on the mechanical properties of the porous samples. The curves exhibited a typical stress–strain curve in which two regions could be distinguished. The first one corresponds to the compression module until the collapse of the scaffold where the slope is low; the second one corresponds to the collapsed structure followed by the collapse of the structure, with a higher slope. The apparent Young modulus calculated from the slope of the stress–strain curve and with the initial cross-sectional area can be obtained for both regions. In what follows, they are named scaffold elastic modulus and collapsed elastic modulus, respectively. Five replicates of each of the samples before HAp growth, with a diameter of 4 mm and a height between 3 and 4 mm, were studied using a universal Microtest compression machine. The strain rate was 1 mm/min, and the load cell used was 15 N.

2.8. Differential Scanning Calorimetry. To identify changes in thermodynamic variables, DSC was used in a Perkin Elmer DSC8000 calorimeter equipped with an intracooler system. The temperature of the equipment was calibrated with water and indium. The melting heat of indium was used for calibrating the heat flow. The calorimeter cells were purged with nitrogen gas at 20 mL/min. The scaffolds of ∼4 mg were encapsulated and subjected to a temperature program consisting of cooling and heating cycles from −10 to 100 °C with a cooling and heating rate of 20 °C/min.

2.9. Statistical Analysis. Data were expressed as mean ± standard deviation. Statistical comparisons were carried out with a one-way analysis of variance (ANOVA). For all analyses, $p < 0.05$ was considered statistically significant. When significant differences were found, a two-tailed Student's t-test was performed. In graphs, the bars represent the standard deviation, and the asterisk indicates that there are statistically significant differences.

https://doi.org/10.1021/acsomega.2c07656
ACS Omega 2023, 8, 7904−7912

3. RESULTS AND DISCUSSION

3.1. Morphology and Ultra-Porous Structure of the Scaffolds. Figure 1 represents the visual examination of pure PCL and PCL-GO scaffolds of 4 mm in diameter and ~3.5 mm in height. The surface texture of the scaffolds was slightly varied according to the composition. While pure PCL scaffold was seen to be white, composite PCL/GO samples showed a uniform dark color, which became deeper as the GO concentration increased. The macroporosity and interconnected pore structure, which facilitate the cell attachment and proliferation of all the scaffolds, are visible.

GO platelets were observed by TEM (see Supporting Information). According to the measurements, the mean surface of an individual platelet is around 0.4 μm^2 and the mean lateral size is about 700 nm.

The scaffold micrographs using FESEM are shown in Figure 2 where its well-defined internal geometry and its uniform pore

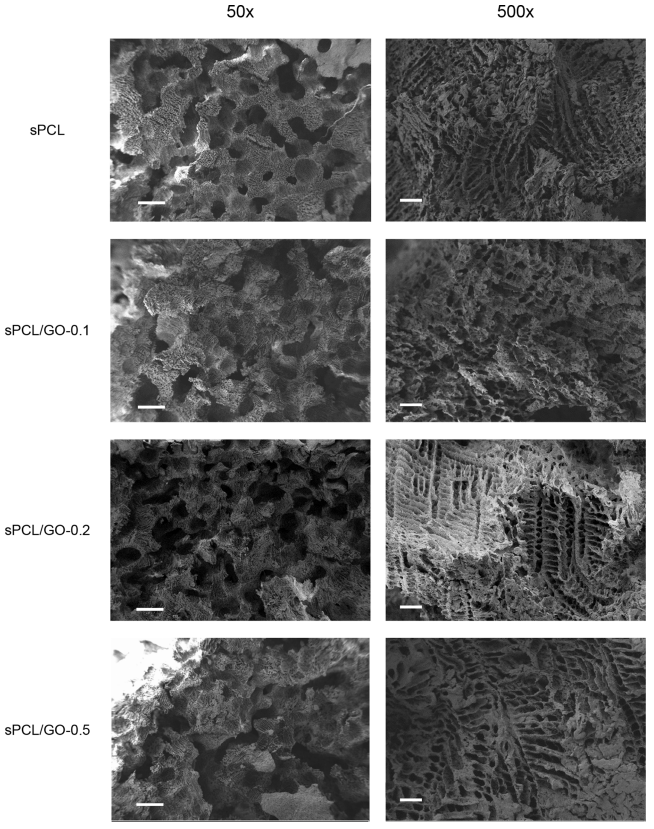

Figure 2. FESEM micrographs of the scaffolds. Scale bar represents 200 μm (left) and 20 μm (right).

distribution can be observed. The porous architecture has a macroporosity of around 200 μm due to the dissolution of the porogen spheres and a microporosity of channels with a pore size of approximately 10 μm as a result of the removal of dioxane by freeze extraction. Microporosity provides samples with a very high specific surface, while macropores allow colonization of the sample by cells. The high porosity and interconnectivity allow diffusion of fluids and nutrients, which help cell metabolism and favor tissue remodeling.[53]

The overall porosity obtained from scaffolds before HAp growth was around 90%. Although the porosity of the pure PCL scaffolds was slightly higher than that of composite scaffolds (see Table 1), no statistical differences were found between samples. These high porosity values make these materials ideal candidates for cell in-growth.

Table 1. Sample Porosity, Mean ± Standard Deviation, as a Function of GO Content

sample	porosity ± SD
sPCL	92.4% ± 1.7%
sPCL/GO-0.1	91.3% ± 2.0%
sPCL/GO-0.2	91.4% ± 2.5%
sPCL/GO-0.5	90.4% ± 2.3%

3.2. Gel Permeation Chromatography. GPC results showed minor mass average molecular weight changes that did not present a clear tendency beyond possible variations in measurements (Table 2). Some authors[54,55] have found a slight increase in the average molecular weight of the composites PCL/GO. However, in our previous studies, where the sonication method was less intense, a decrease in molecular weight with the GO content was observed.[24,50] This can be attributed to the fact that GO sizes decisively influence the conformation of the macromolecular coil. In the work presented here, after the intense sonication process, the sizes of the GO are of the nanometric order (see Supporting Information). When the hybrid dissolves in THF for performing the GPC measurements, GO separates from the macromolecules of the PCL, so the molecular weight is not affected. This result aligns with the analysis by FTIR, indicating a very weak interaction between nano-GO and PCL chains. Likewise, there are no significant differences in the polydispersity indexes, indicating that the size distribution of macromolecular chains remains unchanged.

Table 2. Molecular Weight, M_w, Polydispersity Index, PI, as a Function of GO Content

sample	M_w/Da	PI
sPCL	48,100	1.66
sPCL/GO-0.1	48,960	1.71
sPCL/GO-0.2	45,400	1.89
sPCL/GO-0.5	52,700	1.79

3.3. Mechanical Analysis. Stress−strain curves were obtained from the mechanical compression tests' measured data. Figure 3 shows, as a way of example, the stress−strain curve measured for one of the sPCL replicates and one of the sPCL/GO-0.5 replicates. In these curves, two regions can be appreciated: a first region where the scaffold's collapse occurs and a second region where the elastic deformation of the bulk

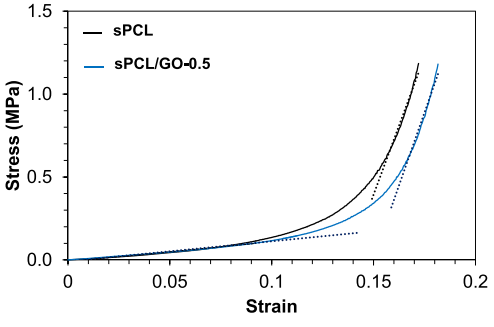

Figure 3. Stress−strain curves for sPCL and sPCL/GO-0.5.

https://doi.org/10.1021/acsomega.2c07656
ACS Omega 2023, 8, 7904−7912

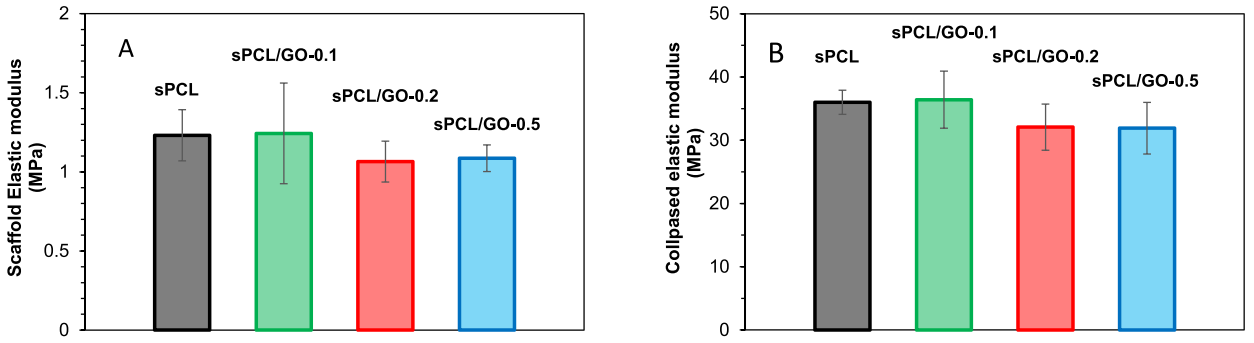

Figure 4. Elastic modulus of the samples: porous part (A) and collapsed scaffold (B).

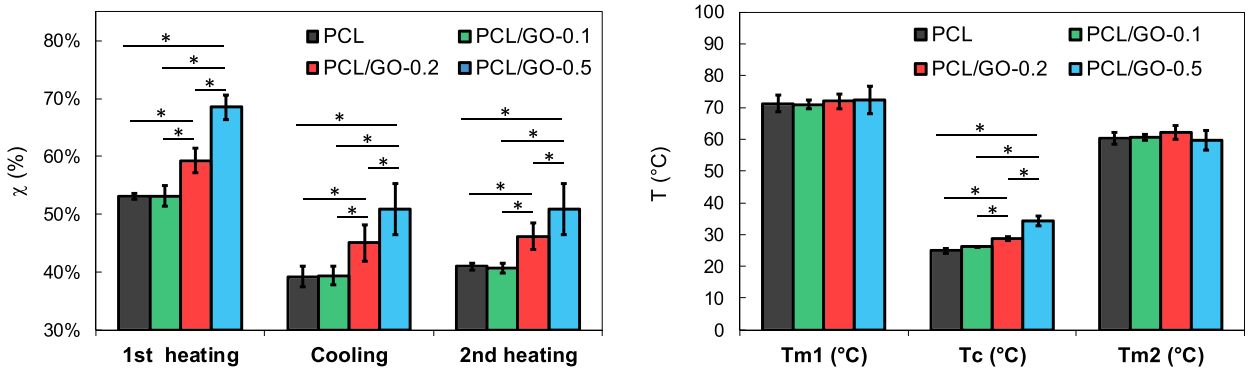

Figure 5. Crystallinity (left) and melting and crystallization temperatures (right) as a function of GO content.

material occurs. These two differentiated regions are characteristic of porous materials, as is the case of the ones studied in this work. From the curves, the apparent elastic modulus values were obtained through a linear fit of the two linear regions (dotted lines in Figure 3). The slope of the curve in the first region represents the apparent elastic modulus of the porous scaffold, and it depends on the Young modulus of the material and on the porosity. The slope of the second region, once the porous structure has collapsed, corresponds to the apparent Young modulus of the material. It is an apparent elastic modulus because the area is changing, and it has not been measured constantly, but the initial value has been taken.

The values of the elastic modulus of the two regions of the stress−strain curves are shown in Figure 4. No statistical differences were found between the moduli of the samples, neither the elastic nor the collapsed. Therefore, the addition of GO does not produce a significant increase or decrease in the PCL scaffolds' compressive modulus, indicating no interaction between the matrix and the filler. Similar results were obtained by Unagolla and Jayasusriya in PCL-GO scaffolds fabricated by an extrusion-based 3D printer,[56] showing that porosity has more influence on the elastic modulus than the filler. However, other authors found a strengthening of the elastic modulus when GO was added, and tensile tests instead of compression tests were performed.[31−33,51]

3.4. Differential Scanning Calorimetry. The samples' thermograms are given in the Supporting Information. Figure 5 shows the scaffold crystallinity (left) and melting and cooling temperatures (right) as a function of GO content. It can be observed that crystallinity (χ) increases with GO addition. Thus, for the first heating, a remarkable increase of 29% should be noted between sPCL (53.02% ± 0.54) and sPCL/GO-0.5 (68.6% ± 2.1). The statistical analysis for the crystallinity obtained during the first heating, cooling, and second heating showed no significant differences between sPCL and sPCL/GO-0.1, but significant differences were found between sPCL and sPCL/GO-0.1 and the rest of the samples.

Similar results have been reported in previous studies[54] in which authors concluded that GO nanoplatelets act as nucleating agents, favoring the formation of crystallization nuclei and therefore increasing the crystallization rate. However, other authors have found that crystallinity decreased when adding GO.[31,32,51] The authors explain the reduction in crystallinity (χ) by the interfacial interaction between PCL molecular chains and GO nanoplatelets, which reduces chain flexibility and recede crystallization, even though GO provides heterogeneous nuclei for PCL crystallization.

Regarding the melting temperatures, the results of Figure 5 (right) show that the addition of GO does not produce a significant variation of T_m either in the first heating or in the second one, which corroborates previous results.[24,57,58] This fact could be attributed to the thickness of the crystals which are almost the same independently of the GO content. On the other hand, the results also show a significant increase in crystallization temperature, T_c, with the addition of GO, which confirms the nucleation effect of GO.

3.5. HAp Deposition: Surface Analysis of the Scaffolds. Some works have indicated the need to improve PCL bioactivity by adding some fillers.[32,34] To analyze the effect of GO on promoting bioactivity, samples were immersed in 5 × SBF. The HAp deposition was characterized by comparison of FTIR spectra of the sample's surface, before and after immersion.

3.5.1. Before Immersion. sPCL and the hybrids before HAp deposition were studied in our previous work.[24] Briefly, marked peaks of sPCL and the hybrids were found around 2800−2900 cm^{-1} due to the asymmetric/symmetric stretch CH_2, a significant peak on 1721 cm^{-1} corresponding to the

https://doi.org/10.1021/acsomega.2c07656
ACS Omega 2023, 8, 7904−7912

C═O stretch of the ester bond and about 1200 cm^{-1} due to the asymmetric stretching C−O−C. No significant spectra differences were observed before SBF immersion with the GO addition.

Furthermore, spectra of the samples before immersion in SBF were resolved based on three Laurentzian-shaped absorption bands[24] attributed to carboxyl absorption bands of amorphous phase, crystalline phase, and hydrogen bonds.[32,55,59] For the sake of comparison, numerical results of the normalized intensity of the three bands are shown in Table 3.

Table 3. Normalized Intensity of the Carboxyl Absorption Band Decomposition at 1734, 1721, and 1700 cm^{-1}

	amorphous	crystalline	H-bonding
sPCL	13.33%	81.04%	5.63%
sPCL/GO-0.1	13.91%	80.65%	5.45%
sPCL/GO-0.2	10.50%	84.83%	4.66%
sPCL/GO-0.5	10.97%	83.95%	5.08%

Results before immersion show that adding GO does not affect the H-bonding, in accordance with GPC results, clearly revealing a poor interaction between nano-GO flakes and PCL. Finally, GO increases the crystallinity as the content increases in accordance with DSC results.

3.5.2. After Immersion. It is worth noting that, after immersion in SBF, the characteristic peaks of the PCL decrease in intensity, Figure 6. Specifically, the peak at 1721 cm^{-1} decreases progressively as the time in immersion increases. This fact is due to the growth of a ceramic layer on the surface of the polycaprolactone, as is seen in FESEM (Figure 8). Thus, the growth kinetics of the said layer can be analyzed, which is reflected in Figure 7. In it, the area under the peak at 1721 cm^{-1} was analyzed as a function of the GO content and the immersion time. The values were normalized for each sample to the area before immersion in SBF. The growth of a ceramic layer is observed on the materials, but it is remarkable that their growth kinetics and the amount of the surface covered (the decrease in the area under the peak) are different. Specifically, the 0.1% graphene oxide sample shows a faster and greater growth than the rest. The decrease in the area under

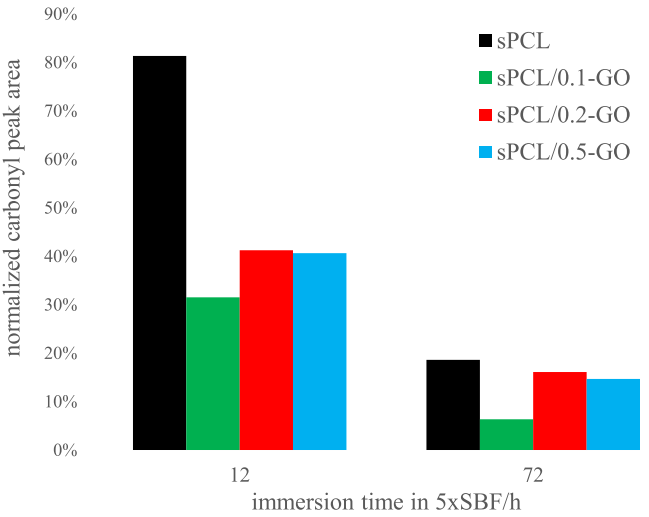

Figure 7. Normalized peak area at 1721 cm^{-1} as a function of immersion time.

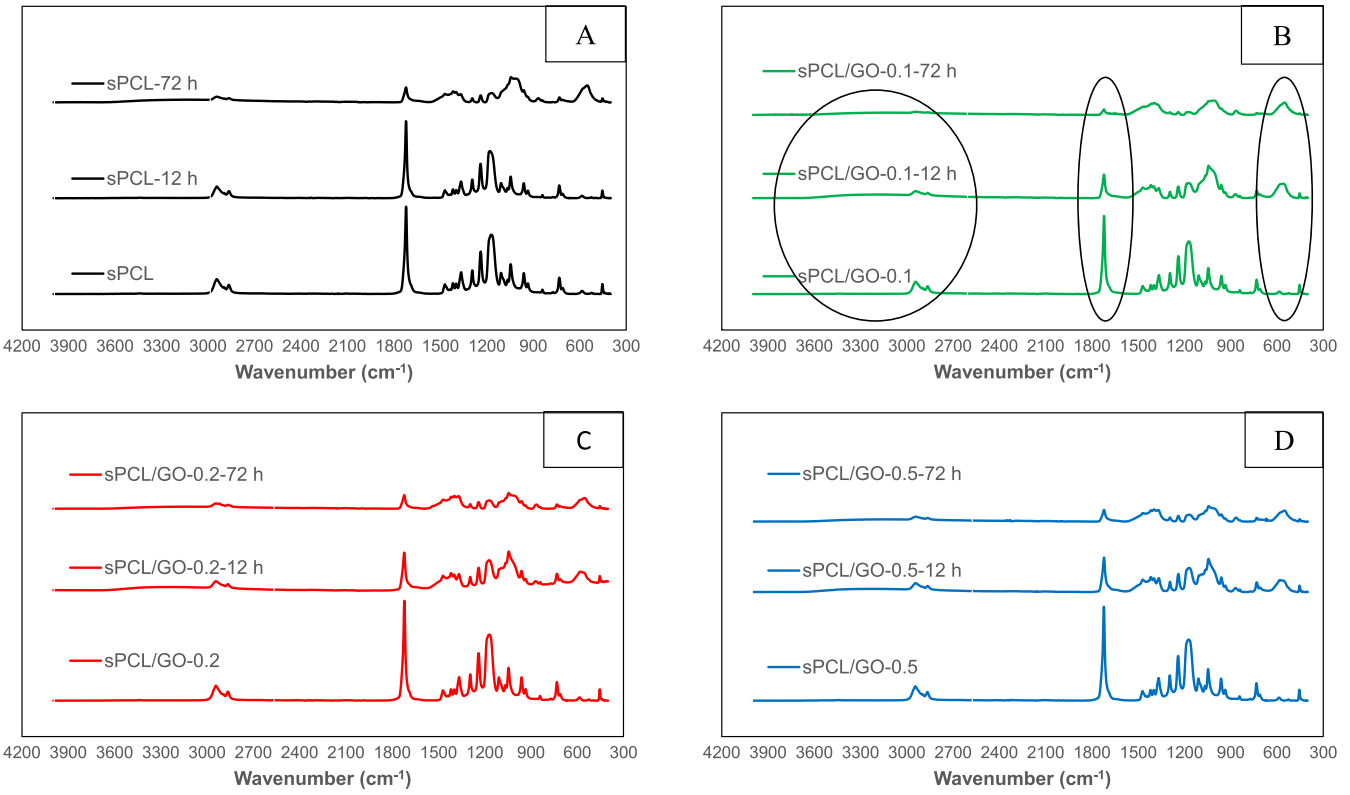

Figure 6. FTIR spectra of the sPCL (A), sPCL/GO-0.1 (B), sPCL/GO-0.2 (C), and sPCL/GO-0.5 (D) scaffolds before and after HAp deposition for 12 and 72 h of 5 × SBF immersion.

https://doi.org/10.1021/acsomega.2c07656
ACS Omega 2023, 8, 7904−7912

the peak can also be correlated with the polymer surface covered by the ceramic layer. Thus, for a period of 72 h, the 0.1% GO sample has reduced the peak area to 6% with respect to its initial value, so the ceramic layer practically covered the sample. However, in the rest of the samples, the area shows a reduction of around 20% for neat polycaprolactone and 15% for the samples of 0.2 and 0.5% GO. Also, it should be noted that the addition of GO induces a faster growth in the ceramic layer. Indeed, it can be observed that at 12 h in immersion, the pure polycaprolactone presents an area under the peak of 81% (little surface covered by the ceramic coating); the samples of 0.2 and 0.5% GO show an area of around 40%, while the sample of 0.1% GO shows an area of ∼32%, which confirms a higher ceramic layer formation kinetics. That the 0.1% GO sample presents more accelerated kinetics and greater growth of the ceramic layer is in line with some results[55] where the mechanical properties reach a maximum for that composition.

Also, the area around 550 cm^{-1} is worth highlighting, where the appearance of a broad peak can be observed in all samples, probably due to the superposition of several peaks which are related to the vibration of the PO_4^{3-} group, characteristic of calcium phosphates. Also, the asymmetric stretching mode of the said group can be observed in the region of 980 to 1250 cm^{-1}. In addition, in the area of 3500−3800 cm^{-1}, a slight bulge can be seen in the spectra as the immersion time increases, characteristic of hydroxyl groups.

Results show that the mineral deposition increased with the immersion time. The FTIR analysis demonstrated the presence of OH^- groups in the samples, whose negative charge can attract calcium ions, in turn, capable of attracting phosphate groups, facilitating the formation of nucleation centers and the growth of calcium phosphates.

This nucleation in the presence of concentrations of ions produced the formation of calcium phosphates in the crystalline HAp phase as could be verified by FESEM. The micrographs in Figure 8 show that HAp deposition in the samples immersed in 5 × SBF was very efficient. Only 12 h after immersion, the samples presented a surface uniformly covered by the biomimetic HAp layer, formed by HAp agglomerates with the typical cauliflower form of this compound. It can be observed that a HAp coat was formed on the internal pore walls of the scaffold, verifying that the high concentration of the 5 × SBF solution induced a fast and uniform deposition of HAp on the nanocomposite scaffolds. The nucleation of HAp covered the surface of the samples' micropores, while its macroporous structure remained unchanged.

In all cases, the formation of HAp agglomerates was observed, giving rise to the characteristic cauliflower structure associated with apatite. The FESEM results show that the HAp crystal size did not show a clear trend. sPCL/GO-0.1 showed the highest crystals, but when the GO content increased, the crystal size decreased to the values of the order of sPCL. In addition, this behavior is similar after 12 and 72 h.

The EDX results obtained for the PCL and PCL-GO scaffolds allowed us to verify that the Ca/P ratios were around 1.68−1.89 (see Supporting Information); that is to say, the Ca/P ratios were, in all cases, close to the stoichiometric HAp. This is the confirmation that the accelerated biomimetic process may be a potential option to achieve the desired HAp deposition, shortening the incubation time in 5 × SBF without compromising the properties of the substrates.

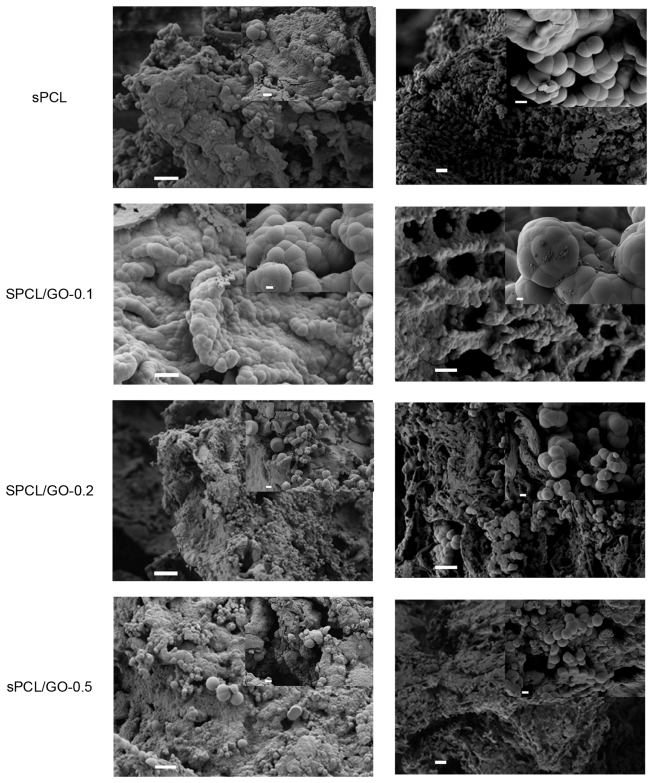

Figure 8. FESEM micrographs of PCL and PCL/GO composite samples after 12 h in 5 × SBF (left) and 72 h (right). Scale bar represents 10 and 1 μm (inset).

4. CONCLUSIONS

The solvent-casting/particulate leaching method was used to synthesize composite scaffolds of PCL with different GO filler contents (0.1, 0.2, and 0.5 wt %). The materials obtained, with a highly interconnected macro- and microporous structure suitable for cell proliferation and tissue regeneration, had an overall porosity of around 90%. Mechanical properties, porosity, and FTIR analysis revealed that the addition of GO did not significantly modify the properties of pristine PCL, indicating that the dispersion of the small amount of sonicated GO had a phantom effect. Thermal characterization showed that the melting temperature of PCL/GO scaffolds was almost unchanged. At the same time, the crystallinity gradually increased with the percentage of GO, as well as the crystallization temperature, which corroborates the nucleation effect of GO.

Moreover, biomimetic treatments on prepared PCL/GO scaffolds disclosed that they had the ability to form HAp in the SBF solution. GO acted as a nucleation point for the HAp crystals having a catalytic effect on HAp, mainly the sample with 0.1%GO, sPCL/GO-0.1, where the effect is more pronounced. Using a concentrated SBF resulted in rapid growth of apatite on the surface of the materials, allowing integration with the host's bone thanks to its bioactive and biocompatible character. Consequently, the results lead us to believe that these biocomposite materials can be promising in bone tissue regeneration.

■ ASSOCIATED CONTENT

Supporting Information

The Supporting Information is available free of charge at https://pubs.acs.org/doi/10.1021/acsomega.2c07656.

https://doi.org/10.1021/acsomega.2c07656
ACS Omega 2023, 8, 7904−7912

TEM image of GO after ultrasonication; DSC thermograms as a function of GO content; and EDX spectra as a function of GO content (PDF)

AUTHOR INFORMATION

Corresponding Author

A.J. Campillo-Fernández − *Centre for Biomaterials and Tissue Engineering, CBIT, Universitat Politècnica de València, 46022 València, Spain;* orcid.org/0000-0002-2978-5994; Phone: +34 963877000 (ext. 88929); Email: alcamfer@ter.upv.es

Authors

S. Fuster-Gómez − *Centre for Biomaterials and Tissue Engineering, CBIT, Universitat Politècnica de València, 46022 València, Spain*

I. Castilla Cortázar − *Centre for Biomaterials and Tissue Engineering, CBIT, Universitat Politècnica de València, 46022 València, Spain*

A. Vidaurre − *Centre for Biomaterials and Tissue Engineering, CBIT, Universitat Politècnica de València, 46022 València, Spain; CIBER de Bioingeniería, Biomateriales y Nanomedicina, Instituto de Salud Carlos III, 28029 Madrid, Spain*

Complete contact information is available at: https://pubs.acs.org/10.1021/acsomega.2c07656

Notes

The authors declare no competing financial interest.

ACKNOWLEDGMENTS

The authors are grateful for the support of the Spanish Ministry of Science, Innovation and Universities through (i) PID2021-126612OB-I00 and (ii) PID2019-106099RB-C41. Also, this research was supported by (iii) CIBER -Consorcio Centro de Investigación Biomédica en Red- (CB06/01/1026), Instituto de Salud Carlos III, Ministerio de Ciencia e Innovación and (iv) H2020 FET-OPEN grant 964562. FESEM images were taken by the authors at the Microscopy Service of the Universitat Politècnica de València, whose advice is greatly appreciated.

REFERENCES

(1) Vacanti, J. P.; Langer, R. Tissue Engineering: The Design and Fabrication of Living Replacement Devices for Surgical Reconstruction and Transplantation. *Lancet* **1999**, *354 Suppl 1*, SI32−SI34.

(2) Langer, R. Biomaterials for Drug Delivery and Tissue Engineering. *MRS Bull.* **2006**, *31*, 477−485.

(3) Mano, J. F. Designing Biomaterials for Tissue Engineering Based on the Deconstruction of the Native Cellular Environment. *Mater. Lett.* **2015**, *141*, 198−202.

(4) Hutmacher, D. W. Scaffolds in Tissue Engineering Bone and Cartilage. *Biomaterials* **2000**, *21*, 2529−2543.

(5) Joseph, J.-G. Polymers for Tissue Engineering, Medical Devices, and Regenerative Medicine. Concise General Review of Recent Studies. *Polym. Adv. Technol.* **2006**, *17*, 395−418.

(6) Hutmacher, D. W.; Schantz, T.; Zein, I.; Ng, K. W.; Teoh, S. H.; Tan, K. C. Mechanical Properties and Cell Cultural Response of Polycaprolactone Scaffolds Designed and Fabricated via Fused Deposition Modeling. *J. Biomed. Mater. Res.* **2001**, *55*, 203−216.

(7) Badylak, S. F.; Freytes, D. O.; Gilbert, T. W. Reprint of: Extracellular Matrix as a Biological Scaffold Material: Structure and Function. *Acta Biomater.* **2015**, *23*, S17−S26.

(8) Yang, X. B.; Bhatnagar, R. S.; Li, S.; Oreffo, R. O. C. Biomimetic Collagen Scaffolds for Human Bone Cell Growth and Differentiation. *Tissue Eng.* **2004**, *10*, 1148−1159.

(9) Williams, J. M.; Adewunmi, A.; Schek, R. M.; Flanagan, C. L.; Krebsbach, P. H.; Feinberg, S. E.; Hollister, S. J.; Das, S. Bone Tissue Engineering Using Polycaprolactone Scaffolds Fabricated via Selective Laser Sintering. *Biomaterials* **2005**, *26*, 4817−4827.

(10) Woodruff, M. A.; Hutmacher, D. W. The Return of a Forgotten Polymer - Polycaprolactone in the 21st Century. *Prog. Polym. Sci.* **2010**, *35*, 1217−1256.

(11) Meseguer-Dueñas, J. M.; Más-Estellés, J.; Castilla-Cortázar, I.; Escobar Ivirico, J. L.; Vidaurre, A. Alkaline Degradation Study of Linear and Network Poly(ε-Caprolactone). *J. Mater. Sci. Mater. Med.* **2011**, *22*, 11−18.

(12) Más Estellés, J.; Vidaurre, A.; Meseguer Dueñas, J. M.; Castilla Cortázar, I. Physical Characterization of Polycaprolactone Scaffolds. *J. Mater. Sci. Mater. Med.* **2008**, *19*, 189−195.

(13) Siddiqui, N.; Asawa, S.; Birru, B.; Baadhe, R.; Rao, S. PCL-Based Composite Scaffold Matrices for Tissue Engineering Applications. *Mol. Biotechnol.* **2018**, *60*, 506−532.

(14) Ghosal, K.; Manakhov, A.; Zajícková, L.; Thomas, S. Structural and Surface Compatibility Study of Modified Electrospun Poly(ε-Caprolactone) (PCL) Composites for Skin Tissue Engineering. *AAPS PharmSciTech* **2017**, *18*, 72−81.

(15) Ghosal, K.; Thomas, S.; Kalarikkal, N.; Gnanamani, A. Collagen Coated Electrospun Polycaprolactone (PCL) with Titanium Dioxide (TiO_2) from an Environmentally Benign Solvent: Preliminary Physico-Chemical Studies for Skin Substitute. *J. Polym. Res.* **2014**, *21*, 410.

(16) Ambekar, R. S.; Kandasubramanian, B. Progress in the Advancement of Porous Biopolymer Scaffold: Tissue Engineering Application. *Ind. Eng. Chem. Res.* **2019**, *58*, 6163−6194.

(17) Chen, B.; Evans, J. R. G. Poly (ε-Caprolactone) - Clay Nanocomposites: Structure and Mechanical Properties. *Macromolecules* **2006**, *39*, 747−754.

(18) Boujemaoui, A.; Cobo Sanchez, C.; Engström, J.; Bruce, C.; Fogelström, L.; Carlmark, A.; Malmström, E. Polycaprolactone Nanocomposites Reinforced with Cellulose Nanocrystals Surface-Modified via Covalent Grafting or Physisorption: A Comparative Study. *ACS Appl. Mater. Interfaces* **2017**, *9*, 35305−35318.

(19) Roseti, L.; Parisi, V.; Petretta, M.; Cavallo, C.; Desando, G.; Bartolotti, I.; Grigolo, B. Scaffolds for Bone Tissue Engineering: State of the Art and New Perspectives. *Mater. Sci. Eng. C Mater. Biol. Appl.* **2017**, *78*, 1246−1262.

(20) Mohammadi, S.; Shafiei, S. S.; Asadi-Eydivand, M.; Mahmoud Ardeshir, M. S.-H. Graphene Oxide-Enriched Poly(ε-Caprolactone) Electrospun Nanocomposite Scaffold for Bone Tissue Engineering Applications. *J. Bioact. Compat. Polym.* **2017**, *32*, 300.

(21) Botlhoko, O. J.; Ray, S. S.; Ramontja, J. Influence of Functionalized Exfoliated Reduced Graphene Oxide Nanoparticle Localization on Mechanical, Thermal and Electronic Properties of Nanobiocomposites. *Eur. Polym. J.* **2018**, *102*, 130−140.

(22) Punetha, V. D.; Rana, S.; Yoo, H. J.; Chaurasia, A.; McLeskey, J. T.; Ramasamy, M. S.; Sahoo, N. G.; Cho, J. W. Functionalization of Carbon Nanomaterials for Advanced Polymer Nanocomposites: A Comparison Study between CNT and Graphene. *Prog. Polym. Sci.* **2017**, *67*, 1−47.

(23) Lebourg, M.; Suay Antón, J.; Gomez Ribelles, J. L. Characterization of Calcium Phosphate Layers Grown on Polycaprolactone for Tissue Engineering Purposes. *Compos. Sci. Technol.* **2010**, *70*, 1796−1804.

(24) Castilla-Cortázar, I.; Vidaurre, A.; Marí, B.; Campillo-Fernández, A. J. Morphology, Crystallinity, and Molecular Weight of Poly(ε-Caprolactone)/Graphene Oxide Hybrids. *Polymers (Basel)* **2019**, *11*, 1099.

(25) Novoselov, K.S.; Geim, A. K.; Morozov, S. V.; Jiang, D.; Zhang, Y.; Dubonos, S. V.; Grigorieva, I. V.; Firsov, A. A. Electric field effect in atomically thin carbon films. *Science* **2004**, *306* (5696), 666−669.

(26) Dreyer, D. R.; Park, S.; Bielawski, C. W.; Ruoff, R. S. Graphite Oxide. *Chem. Soc. Rev.* **2010**, *39*, 228−240.
(27) Ghosal, K.; Sarkar, K. Biomedical Applications of Graphene Nanomaterials and Beyond. *ACS Biomater. Sci. Eng.* **2018**, *4*, 2653−2703.
(28) Wu, C.; Xia, L.; Han, P.; Xu, M.; Fang, B.; Wang, J.; Chang, J.; Xiao, Y. Graphene-Oxide-Modified Beta-Tricalcium Phosphate Bioceramics Stimulate in Vitro and in Vivo Osteogenesis. *Carbon* **2015**, *93*, 116−129.
(29) Song, J.; Gao, H.; Zhu, G.; Cao, X.; Shi, X.; Wang, Y. The Preparation and Characterization of Polycaprolactone/Graphene Oxide Biocomposite Nanofiber Scaffolds and Their Application for Directing Cell Behaviors. *Carbon* **2015**, *95*, 1039−1050.
(30) Sayyar, S.; Murray, E.; Thompson, B. C.; Gambhir, S.; Officer, D. L.; Wallace, G. G. Covalently Linked Biocompatible Graphene/Polycaprolactone Composites for Tissue Engineering. *Carbon* **2013**, *52*, 296−304.
(31) Kai, W.; Hirota, Y.; Hua, L.; Inoue, Y. Thermal and Mechanical Properties of a Poly(ε-Caprolactone)/Graphite Oxide Composite. *J. Appl. Polym. Sci.* **2008**, *107*, 1395−1400.
(32) Wan, C.; Chen, B. Poly(ε-Caprolactone)/Graphene Oxide Biocomposites: Mechanical Properties and Bioactivity. *Biomed. Mater.* **2011**, *6*, No. 055010.
(33) Lopresti, F.; Maio, A.; Botta, L.; Scaffaro, R. Preparation and Mechanical Characterization of Polycaprolactone/Graphene Oxide Biocomposite Nanofibers. *AIP Conf. Proc.* **2016**, *1736*, No. 020105.
(34) Erdal, N. B.; Hakkarainen, M. Construction of Bioactive and Reinforced Bioresorbable Nanocomposites by Reduced Nano-Graphene Oxide Carbon Dots. *Biomacromolecules* **2018**, *19*, 1074−1081.
(35) Hassanzadeh, S.; Adolfsson, K. H.; Wu, D.; Hakkarainen, M. Supramolecular Assembly of Biobased Graphene Oxide Quantum Dots Controls the Morphology of and Induces Mineralization on Poly(ε-Caprolactone) Films. *Biomacromolecules* **2016**, *17*, 256−261.
(36) Yadav, A.; Erdal, N. B.; Hakkarainen, M.; Nandan, B.; Srivastava, R. K. Cellulose-Derived Nanographene Oxide Reinforced Macroporous Scaffolds of High Internal Phase Emulsion-Templated Cross-Linked Poly(ε-Caprolactone). *Biomacromolecules* **2020**, *21*, 589−596.
(37) Akhavan, O.; Ghaderi, E. Toxicity of Graphene and Graphene Oxide Nanowalls against Bacteria. *ACS Nano* **2010**, *4*, 5731−5736.
(38) Daulbayev, C.; Sultanov, F.; Korobeinyk, A. V.; Yeleuov, M.; Taurbekov, A.; Bakbolat, B.; Umirzakov, A.; Baimenov, A.; Daulbayev, O. Effects of Graphene Oxide/Hydroxyapatite Nanocomposite on Osteogenic Differentiation and Antimucrobial Activity. *Surf. Interfaces* **2022**, *28*, No. 101683.
(39) Samavedi, S.; Whittington, A. R.; Goldstein, A. S. Calcium Phosphate Ceramics in Bone Tissue Engineering: A Review of Properties and Their Influence on Cell Behavior. *Acta Biomater.* **2013**, *9*, 8037−8045.
(40) Dorozhkin, S. V. Biphasic, Triphasic and Multiphasic Calcium Orthophosphates. *Acta Biomater.* **2012**, *8*, 963−977.
(41) Khodabandeh, Z.; Tanideh, N.; Sari Aslani, F.; Jamhiri, I.; Zare, S.; Alizadeh, N.; Safari, A.; Farshidfar, N.; Dara, M.; Zarei, M. A Comparative in Vitro and in Vivo Study on Bone Tissue Engineering Potential of the Collagen nano-Hydroxyapatite Scaffolds Loaded with Ginger Extract and Curcumin. *Mater. Today Commun.* **2022**, *31*, No. 103339.
(42) Regina Avanzi, I.; Risso Parisi, J.; Souza, A.; Almeida Cruz, M.; Santi Martignago, C. C.; Araki Ribeiro, D.; Cavalcante Braga, A. R.; Renno, A. C. 3D-printed Hydroxyapatite Scaffolds for Bone Tissue Engineering: A Systematic Review in Experimental Animal Studies. *J. Biomed. Mater. Res. B Appl. Biomater.* **2023**, *111*, 203−219.
(43) Thein-Han, W. W.; Misra, R. D. K. Biomimetic Chitosan−Nanohydroxyapatite Composite Scaffolds for Bone Tissue Engineering. *Acta Biomater.* **2009**, *5*, 1182−1197.
(44) Kokubo, T.; Takadama, H. How Useful Is SBF in Predicting in Vivo Bone Bioactivity? *Biomaterials* **2006**, *27*, 2907−2915.
(45) Bohner, M.; Lemaitre, J. Can Bioactivity Be Tested in Vitro with SBF Solution? *Biomaterials* **2009**, *30*, 2175−2179.
(46) Kim, S. S.; Park, M. S.; Gwak, S. J.; Choi, C. Y.; Kim, B. S. Accelerated Bonelike Apatite Growth on Porous Polymer/Ceramic Composite Scaffolds in Vitro. *Tissue Eng.* **2006**, *12*, 2997−3006.
(47) Stoch, A.; Jastrzębski, W.; Brozek, A.; Stoch, J.; Szaraniec, J.; Trybalska, B.; Kmita, G. FTIR Absorption-Reflection Study of Biomimetic Growth of Phosphates on Titanium Implants. *J. Mol. Struct.* **2000**, *555*, 375−382.
(48) Rezaei, A.; Mohammadi, M. R. In Vitro Study of Hydroxyapatite/Polycaprolactone (HA-PCL) Nanocomposite Synthesized by an in Situ Sol-Gel Process. *Mater. Sci. Eng., C Mater. Biol. Appl.* **2013**, *33*, 390−396.
(49) Hashim, N. C.; Frankel, D.; Nordin, D. Graphene Oxide-Modified Hydroxyapatite Nanocomposites in Biomedical Applications: A Review. *Ceram. Silik.* **2019**, *63*, 426−448.
(50) Campillo-Fernández, A. J.; González-Reed, P.; Vidaurre, A.; Castilla-Cortázar, I. Poly(-Caprolactone)/Graphene Oxide Composite Systems: A Comparative Study on Hydrolytic Degradation at Extreme PH Values. *Mater. Express* **2020**, *10*, 892−902.
(51) Martínez-Ramón, V.; Castilla-Cortázar, I.; Vidaurre, A.; Campillo-Fernández, A. J. Production and Enzymatic Degradation of Poly(ε-Caprolactone)/Graphene Oxide Composites. *Mater. Express* **2020**, *10*, 866−876.
(52) Huang, Y.; Xu, Z.; Huang, Y.; Ma, D.; Yang, J.; Mays, J. W. Characterization of Poly(ε-Caprolactone) via Size Exclusion Chromatography with Online Right-Angle Laser-Light Scattering and Viscometric Detectors. *Int. J. Polym. Anal. Charact.* **2003**, *8*, 383−394.
(53) Ródenas-Rochina, J.; Ribelles, J. L. G.; Lebourg, M. Comparative Study of PCL-HAp and PCL-Bioglass Composite Scaffolds for Bone Tissue Engineering. *J. Mater. Sci. Mater. Med.* **2013**, *24*, 1293−1308.
(54) Hua, L.; Kai, W. H.; Inoue, Y. Crystallization Behavior of Poly(ε-Caprolactone)/Graphite Oxide Composites. *J. Appl. Polym. Sci.* **2007**, *106*, 4225−4232.
(55) Ramazani, S.; Karimi, M. Aligned Poly(ε-Caprolactone)/Graphene Oxide and Reduced Graphene Oxide Nanocomposite Nanofibers: Morphological, Mechanical and Structural Properties. *Mater. Sci. Eng., C Mater. Biol. Appl.* **2015**, *56*, 325−334.
(56) Unagolla, J. M.; Jayasusriya, A. C. Enhanced Cell Functions on Graphene Oxide Incorporated 3D Printed Polycaprolactone Scaffolds. *Mater. Sci. Eng., C Mater. Biol. Appl.* **2019**, *102*, 1−11.
(57) Wang, G. S.; Zhi-yong, W.; Lin, S.; Chen, G.; Zhang, W.; Dong, X.; Qi, M. Morphology, Crystallization and Mechanical Properties of Poly(ε-Caprolactone)/Graphene Oxide Nanocomposites. *Chinese J. Polym. Sci.* **2013**, *31*, 1148−1160.
(58) Yıldırım, S.; Demirtaş, T. T.; Dinçer, C. A.; Yıldız, N.; Karakeçili, A. Preparation of Polycaprolactone/Graphene Oxide Scaffolds: A Green Route Combining Supercritial CO_2 Technology and Porogen Leaching. *J. Supercrit. Fluids* **2018**, *133*, 156−162.
(59) Honma, T.; Senda, T.; Inoue, Y. Thermal Properties and Crystallization Behaviour of Blends of Poly(ε-Caprolactone) with Chitin and Chitosan. *Polym. Int.* **2003**, *52*, 1839−1846.

https://doi.org/10.1021/acsomega.2c07656
ACS Omega 2023, 8, 7904−7912